Case Studies in Construction Materials 19 (2023) e02381

Contents lists available at ScienceDirect

Case Studies in Construction Materials

journal homepage: www.elsevier.com/locate/cscm

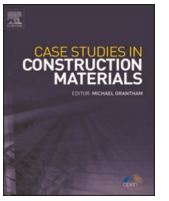

A novel test procedure for evaluating the performance of composite cured-in-place-pipe liners in water pressure pipe rehabilitation

Ferran Gras-Travesset [a,b], Antoni Andreu-Torras [b], Marco A. Pérez [a,*]

[a] IQS School of Engineering, Universitat Ramon Llull, Via Augusta 390, 08017 Barcelona, Spain
[b] Aigües de Barcelona, General Batet, 1-7, Barcelona 08028, Spain

ARTICLE INFO

Keywords:
Trenchless technology
Cured-in-place pipe CIPP
Water pipe rehabilitation
Sewer rehabilitation
Pipe lining
Experimental testing
Inner Balloon Pressure Test IBPT

ABSTRACT

The cured-in-place pipe (CIPP) is a pipe rehabilitation technique that is becoming increasingly popular due to its cost advantages, reduced environmental impact, and decreased time requirements compared to traditional pipe replacement. However, some CIPP rehabilitation projects have revealed deficiencies in predicted liner performance. This paper proposes and validates the Inner Balloon Pressure Test, a new test procedure for the quality control of CIPP rehabilitation liners. The test is intended to replicate the working stress conditions of an installed CIPP liner, and is proposed as an alternative to the curved specimen bending test recommended by the current CIPP standard and which has been shown to overestimate the ultimate stresses of cured CIPP liner specimens by more than 200%. Consequently, in a liner of DN 385 and 6 mm of thickness, a burst pressure of 138.2 bar was predicted through the bending test, whereas 62.8 bar was deducted from tensile tests. The experimental evidence provided in this study can significantly impact the design of CIPP pressure pipe liners. Inadequate sizing of the structural reinforcement can compromise the liner functionality and the rehabilitation of the pipeline. Therefore, this study provides a novel test that reduces uncertainties related to the strength analysis of CIPP liners. Furthermore, it contributes to optimizing and advancing existing design and quality control techniques.

1. Introduction

The quality of the water supply network is essential to ensure a continuous water supply and prevent the loss of potable water during transport from the treatment plant to the consumer. However, the water supply and sewage networks have aged and deteriorated over the years, causing a significant increase in faults as reported in [1]. This is demonstrated in a recent study [2] conducted by the American Society of Civil Engineers (ASCE), which estimated that a water leak occurs every 2 min in the US and that 22.7 hm^3 of potable water is lost daily. The greatest challenge in addressing this problem is the extensive mileage. In 2020, supply lines extended 248,245 km [3] in Spain, 875,000 km [4] in France, and $3.54 \cdot 10^6$ km [2] in the United States.

Rehabilitation techniques have proven to be an alternative to traditional and costly pipe replacement. Rehabilitation rather than replacement is a faster solution, is more cost-effective and environmentally friendly, and significantly reduces the disruption to city

* Corresponding author.
E-mail address: marcoantonio.perez@iqs.url.edu (M.A. Pérez).

https://doi.org/10.1016/j.cscm.2023.e02381
Received 4 March 2023; Received in revised form 26 July 2023; Accepted 5 August 2023
Available online 26 August 2023

activity caused by pipe replacement. The most widely used techniques are spraying, pipe bursting, slip-lining, thermoformed pipe lining (Fold-and-Form), and Cured-In-Place-Pipe (CIPP). Among them, CIPP has expanded considerably in recent years. CIPP is a rehabilitation technique that involves the insertion of an initially soft liner impregnated with resin into a host pipe, as detailed in Section 2. In Germany, rehabilitation with CIPP represented 17.9% of the repair and renovation market in 2020 [5]. It is predicted that in 2023, the global investment in CIPP will be approximately 2615.4 million dollars [6].

Though CIPP is widely used in the wastewater sector, the pressure reached in supply pipes (which can exceed 10 bars) make the rehabilitation process more challenging. As recognized by experts, slight imperfections during installation limit the performance of the rehabilitated pipe. In some cases, even resulting in a pipe going out of service.

Several problems may also arise after installation (see Fig. 1), as stated in [7] where field experiences from four CIPP projects were exposed. The most common installation defects are cracks, longitudinal wrinkles, lack of contact between the host pipe and the liner in semi-structural or non-structural liners, impregnation imperfections, swollen areas due to water drainage between the liner and the host pipe, and wall buckling [8]. For these reasons, rigorous quality control is required during and after installation. According to current standards such as ASTM F1216 [9], EN ISO 11296–4 [10], and ISO 11298–4 [11], quality control tests are based mainly on bending tests of cured samples of the installed liner. However, deficiencies detected in several CIPP rehabilitation projects suggest that the predicted performance estimated by standard tests may not approximate the actual pipe performance. Due to this uncertainty [12], several CIPP market companies are developing specific quality control procedures. However, there is yet to be a consensus on it. Recently, various organizations have started to centralize, unify and standardize these quality control procedures. For example, a standard on CIPP technology (EN ISO 11298–4 [13] and UNE 53929 [14]) was recently developed in Spain.

Researchers have contributed to the current design standards by investigating the CIPP rehabilitation process through experimental testing on the pipes themselves [15–18]. In a pioneering study [16], the six limit states of CIPP were presented, and it was concluded that longitudinal wrinkles significantly affect the mechanical properties of the liner. Allouche et al. [15] addressed the numerical and analytical verification of the burst pressure of a pipe with circular holes between 38.1 and 203.2 mm (1.5–8 in.) presented in the ASTM F2207 standard [19]. The study tested a PVC (Polyvinyl Chloride) pipe reinforced with steel rings to determine the effect of the holes and better understand the long-term behavior of CIPP. The authors concluded that the deformation of the liner during primary fluence was directly related to the size of the circular hole. Other researchers numerically and experimentally investigated the effect of longitudinal wrinkles on the liner and the appearance of holes in the host pipe using laboratory-scale prototypes [17,20]. The authors established that the passage of a wrinkle through a circular hole in the host pipe further decreased the mechanical performance of the installed liner.

The wrinkles in CIPP are classified according to their geometry into SW (i.e. only the inner layer is lifted), IW (i.e. symmetric wrinkle), and LW (i.e. asymmetric wrinkle) [21]. Further research has focused on investigating the reduction of the mechanical properties of sewer CIPP liners in service between 5 and 25 years with a nominal diameter (DN) of 203.2–1219.2 mm (8–48 in.) [22]. In these studies, it has been concluded that reduction in the liner properties was not detected. The authors also highlighted that just four of the tested liners reached half of their life expectancy. In addition, only the first liner installed worldwide has reached 50 years of it's expected life [22]. Moreover, full-scale tests have been consistently investigated [23,24] providing useful data to validate the multiple numerical models found in the literature [18,25,26].

Scientific findings have undoubtedly contributed to the design and improvement of lining pipes and CIPP technology. However, due to the high number of incidents and unsatisfactory rehabilitations, in recent years, there has been a need to establish strict quality controls to ensure that the liner has been correctly installed and meets the specified requirements. Currently, due to its operational simplicity [27], the three-point bending test of cured samples presented in EN ISO 11296–4 [10] is the main quality control test used to assess the tensile performance of CIPP liners.

The flexural test is widely used in the characterization of composite specimens [28–30]. Accordingly, the standard practice for the rehabilitation of existing pipelines (i.e., EN ISO 11296–4 [10] and ISO 11298–4 [13]) has adopted this procedure for the mechanical characterization of CIPP specimens. Nonetheless, the CIPP liners are mainly subjected to tensile loads due to the inner pressure of the pipe. However, the impracticality of extracting flat samples in the hoop direction makes the conventional tensile test unfeasible. Furthermore, the stress state (tensile, compressive, and shear stresses) and failure modes (see Fig. 13) that occur in a sample subjected

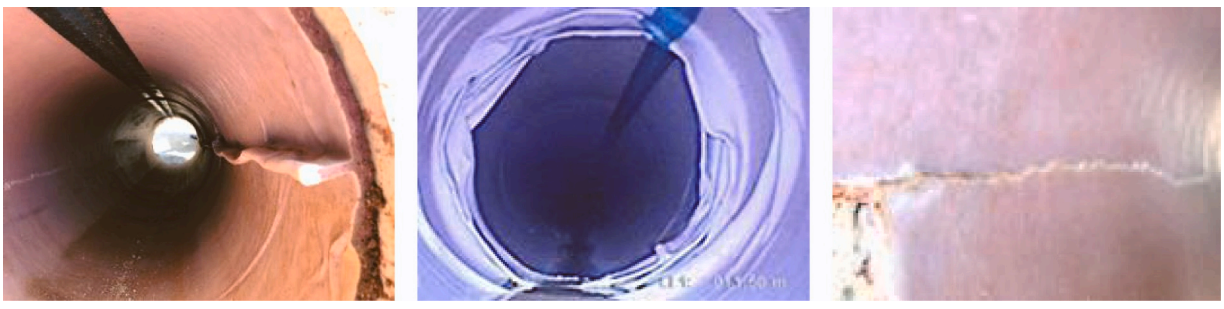

a) b) c)

Fig. 1. Example of defects resulting from improper CIPP installation. a) Longitudinal wrinkle. b) Hoop wrinkles. c) Longitudinal crack.

to flexure are complex [31–33] and different from tensile. Consequently, the bending test could be questionable for assessing the performance of an installed CIPP liner.

Accordingly, this paper proposes and validates a new test procedure for testing ring samples. The Inner Balloon Pressure Test (IBPT), aimed to reproduce the working conditions of a CIPP-installed liner and is proposed as an alternative to the three-point bending test of curved samples recommended by the current CIPP regulations.

2. CIPP design considerations

The advantage of trenchless rehabilitation technologies is that they use the existing pipes as a host taking advantage of their residual mechanical performance. Thus a new pipe is created within the damaged one, with minimal reduction in nominal diameter. There are different rehabilitation techniques, and each has its application and market. Particularly, CIPP is a technique that involves inserting an initially soft and resin-impregnated liner into a host pipe. The liner is a layered composite formed by fibers embedded in a resin matrix that acts as a binding component. An external polymer coating prevents resin migration and fibers from contacting the potable water. Once inserted into the damaged pipe, the liner is expanded by pressure to fit the host pipe and after the resin curing process (by steam or ultraviolet light), the soft lining solidifies, creating a new solid pipe within the host pipe (see Fig. 2).

According to the American Water Works Association (AWWA) [34], CIPP liners are classified as non-structural, semi-structural, or structural. Non-structural liners do not improve the host pipe's structural performance. Hence, they are mainly used to prevent clean water from coming into contact with corrosion from the host pipe. Semi-structural liners can partially withstand internal and external loads, such as small voids, corrosion pits, or joint gaps, but require residual structural contribution from the host pipe. Finally, structural liners are designed to withstand all internal and external loads. Thus, structural liners are used when the host pipe is severely damaged and has lost its structural capacity.

CIPP liners are designed considering the host pipe's residual load-bearing capacity. The technical standard ASTM F1216 [9] provides a detailed dimensioning procedure, defining the minimum performance the liner must achieve once cured to verify that the installation has been completed correctly. The expansion coefficient and burst pressure are critical mechanical properties in CIPP liners. Especially in semi-structural liners, the maximum coefficient of expansion of the uncured liner is crucial because the liner should completely fit the host pipe. The burst pressure is directly proportional (Eq. (1)) to the ultimate stress of the liner in the hoop direction (see Fig. 2):

$$\sigma = \frac{P\,r}{h} \tag{1}$$

where σ is the hoop stress (MPa), P is the internal pressure (MPa), r is the inner radius (mm), and h is the thickness (mm). As stated before, obtaining the tensile standard dog-bone type sample along the hoop direction is unfeasible due to the curved geometry of the cured samples. For this reason, the current technical standard (EN ISO 11296–4 [10]) uses curved shape samples to perform a three-point bending test, as shown in Fig. 3. The tensile stress-strain results can be analytically extrapolated from the bending test, assuming a linear distribution of stresses and strains along the thickness according to Eq. (2), and after applying the curvature correction (Eqs. (5) and (6)) proposed in EN ISO 11296–4 [10].

However, as proven below, the experimental evidence shows that the ultimate stress obtained in the bending test is significantly higher than in the tensile strength test of flat CIPP samples. Therefore, in the authors' opinion, the test can be questioned. Consequently, it is considered necessary to develop, compare and validate a test for curved samples capable of better reproducing the working conditions to which an installed CIPP liner is subjected.

3. Inner Balloon Pressure Test

The new test procedure, called Inner Balloon Pressure Test (IBPT), is proposed as an alternative to the three-point bending test of curved samples recommended by the current standard and aims to reproduce the working stress conditions of a CIPP-installed liner. The IBPT obtains the hoop stress and burst pressure of a ring sample extracted from an installed CIPP liner. The test involves applying

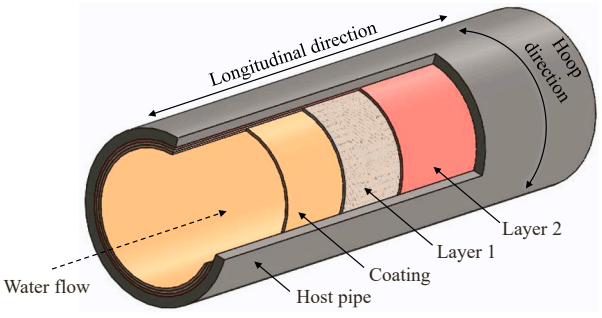

Fig. 2. Representation of a pipeline rehabilitated using CIPP.

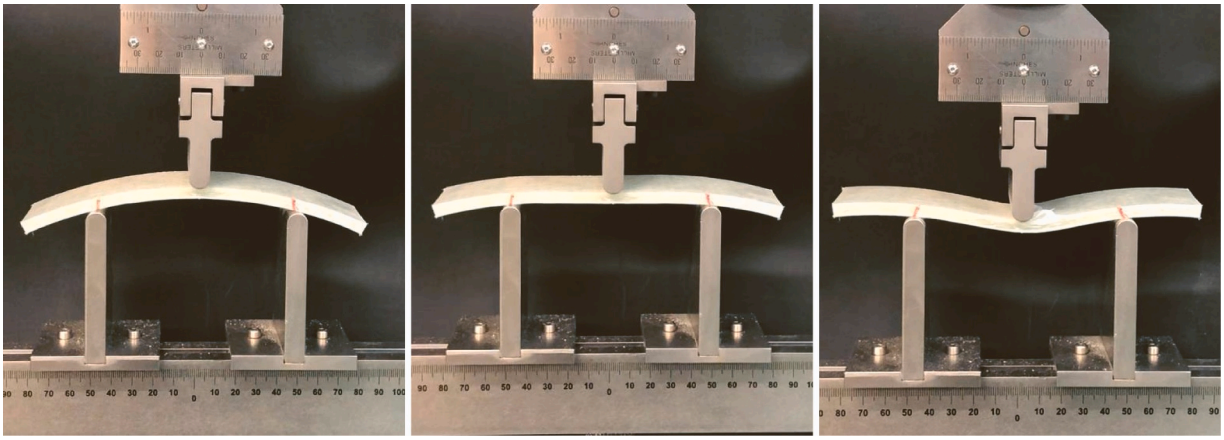

Fig. 3. Experimental setup of a three-point bending test of a cured CIPP sample liner (DN385 mm), according to the technical standard EN ISO 11296–4. [10].

hydrostatic pressure to the ring sample's inner face to obtain the sample's tensile properties in the hoop direction (see Figs. 4 and 5).

The schematic drawing of the test set-up is shown in Figs. 4 and 5. The samples are located between two rigid plates joined by threaded rods to support the internal pressure. The upper plate has a central hole that allows the pressurized fluid to enter and exit. The fluid is introduced into the membrane inside the sample to avoid leakage. Thus, the membrane transfers the hydrostatic pressure to the inner face of the tested ring sample. The test system allows the sample to expand radially by sliding between the two tooling plates. Using lubricant minimized the friction between the sample and the tooling plates.

4. Materials and methods

Firstly, the research methodology was designed to compare the tensile test of CIPP flat samples with the three-point bending test of curved CIPP composite samples to identify the shortcomings of the bending test as a CIPP quality control test. Secondly, the proposed IBPT was validated by comparing the test results with PVC and CIPP composite ring samples, with experimental tensile tests and results from a developed numerical model. Details of materials, samples, test setups and numerical models are given below.

4.1. CIPP liner test samples

The CIPP liner used in this study was of type structural class A according to ISO 11295: 2019 table 16 [35] and class IV according to AWWA CIPP classification [34]. The liner is composed of three layers of fiberglass and a polyethene (PE) coating that prevents fiber migration to the drinking water (see Fig. 2). The resin used was a styrene-free vinyl ester resin with very low VOC (Volatile Organic

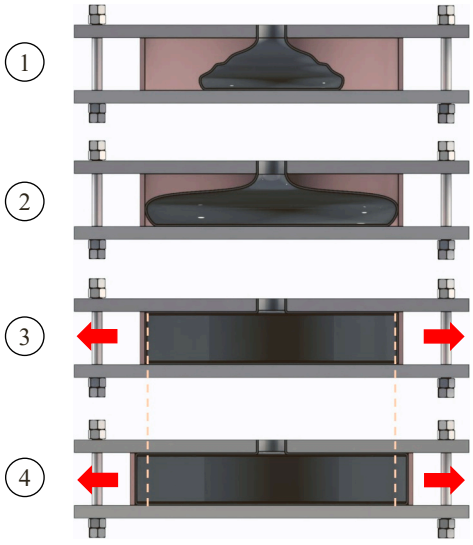

Fig. 4. Schematic drawing of the Inner Balloon Pressure Test (IBPT) setup.

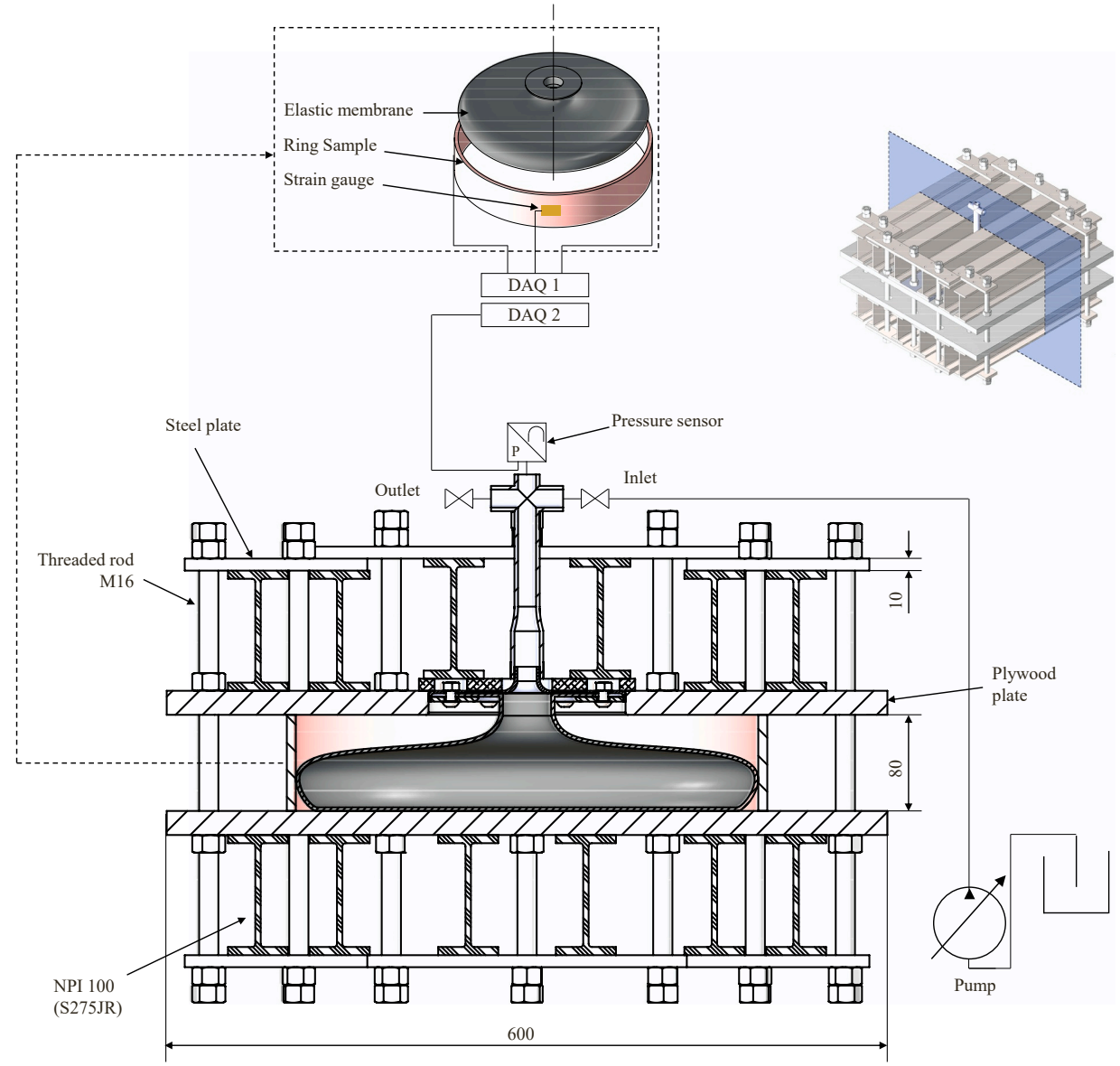

Fig. 5. Assembly drawing of the Inner Balloon Pressure Test (IBPT) setup.

Compound) content, used for CIPP and specific for potable water pipes. A UV curing process solidifies the resin. The liner was first analyzed with a high-resolution Olympus DSX1000 digital microscope (see Fig. 6).

Two different curing processes obtained samples of the cured liner. First, flat samples were cured under controlled laboratory conditions because obtaining flat samples from an installed liner in a cylindrical pipe was unfeasible. These flat laboratory samples were cured by UV lamps type A, B, and C with an exposure time of 2 min. Afterwards, a numerically controlled machining process was used to obtain the type I dog-bone samples according to ASTM D638 [36]. Second, CIPP ring samples were obtained from a rehabilitated DN400 reinforced concrete pipe (Fig. 8) with the same liner. The curing process was performed under real installation conditions using a trolley of 9 UV lamps of 400 W each (see Fig. 7)

4.2. Tensile test

Tensile testing of PVC flat samples and CIPP liner samples was carried out according to ASTM D638 [36] using a type I geometry. Due to the isotropy of PVC material, the PVC tensile samples were obtained by machining a PVC pipe along the longitudinal direction. As stated before, the CIPP liner tensile samples were cured in the laboratory on a flat surface and then machined to obtain flat samples in the hoop direction. Tests were conducted on a ZwickRoell Z30 universal mechanical testing equipment with a 30 kN load cell and a

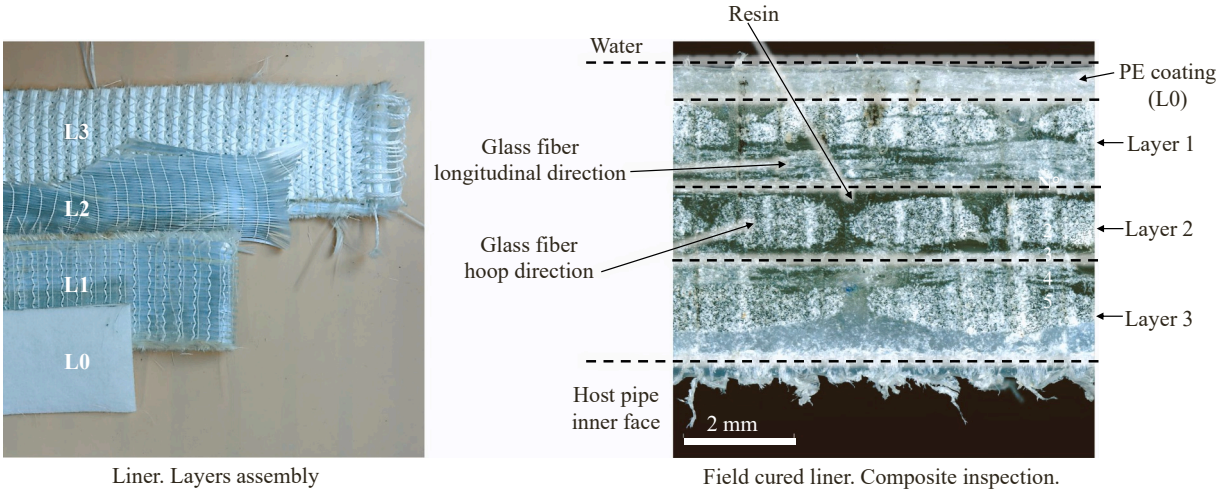

Fig. 6. Arrangement of the CIPP composite liner used.

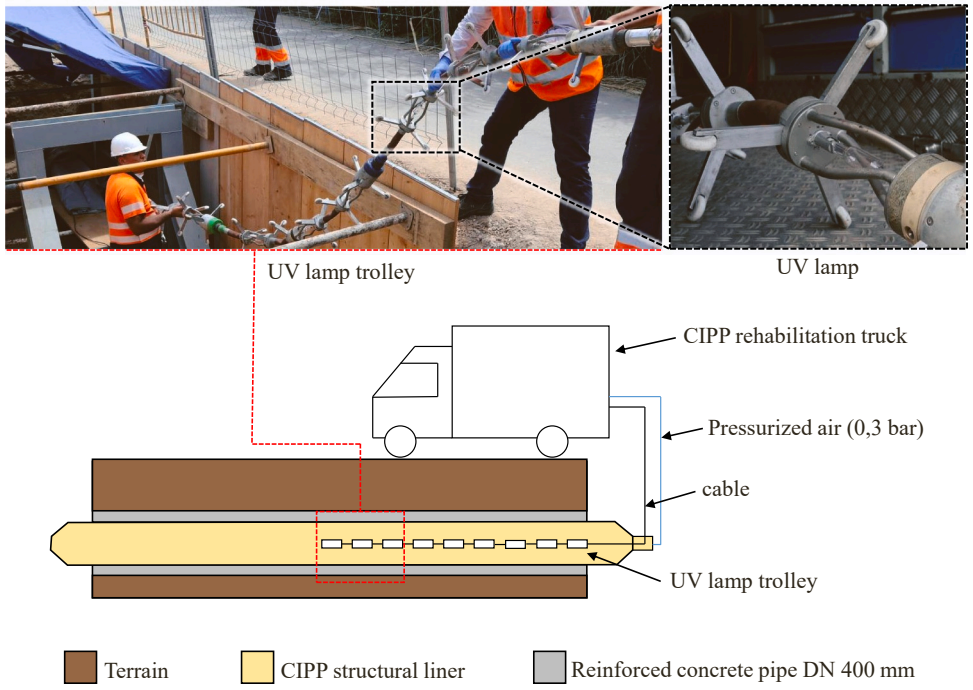

Fig. 7. Field UV and pressure curing process of the installed liner.

50 mm ZwickRoell extensometer. Samples were tested with a preload of 5 N and a test speed of 5 mm/min. Young's modulus was calculated by the regression method between the strain range [0.05–0.25%]. The test speed for calculating the elastic modulus was 1%/min.

4.3. Three-point bending test

Three-point bending tests were performed following EN ISO 11296–4 [10] and ISO 178 [37] on curved samples using the same ZwickRoell Z30 universal mechanical testing equipment. The samples tested had an inner radius of 192.5 mm, a width (b) of 50 mm, and a thickness (h) of approximately 6 mm. The distance between supports (L) was set at 96 mm, so the actual support distance L_2 of the sample was 99.93 mm. The samples were tested according to the standard using a preload of 2 MPa and a test speed of 10 mm/min. The strain rate to calculate the modulus of elasticity was set to 1%/min. Young's modulus was calculated according to Eq. (4) between the strain range [0.05–0.25%], where $\varepsilon_2 = \varepsilon_1 + 2000.10^{-6}$ mm/mm and ε_1 takes the value that maximizes Young's modulus. The

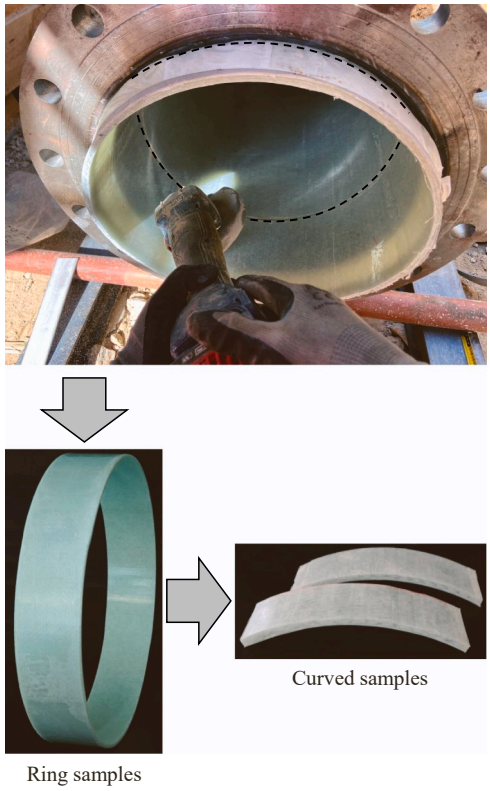

Fig. 8. Extraction of the ring samples of an installed CIPP liner of DN 385 mm.

apparent stress and strain were respectively calculated according to Eqs. (2) and (3):

$$\sigma_c = \frac{3FL_2}{2bh^2} \tag{2}$$

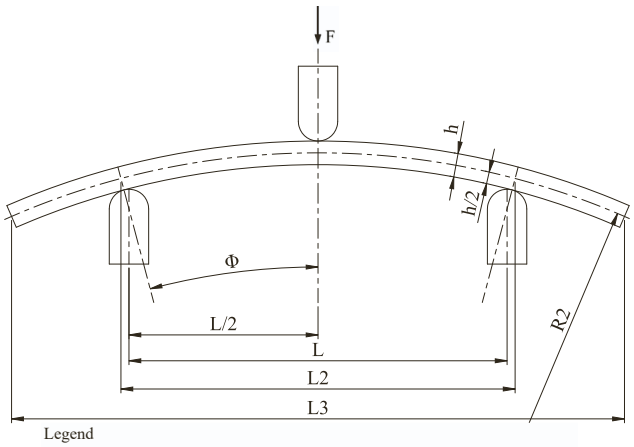

Legend
F: Applied force.
h: Total thickness of the sample.
L: Distance between supports.
L2: Real distance between the supports of a curved sample.
L3: Total length of the chord of a curved sample.
R2: Radius of curvature of the sample at half the thickness
Φ: Half-angle of an unloaded specimen formed between the actual contact points of the supports.

Fig. 9. Three-point bending test scheme of a curved sample according to EN ISO 11296–4 [10].

where σ_c is the apparent stress of a curved sample subjected to bending before the curvature correction (MPa), F is the applied force (N), L_2 is the actual distance between the supports of a curved sample subjected to bending (mm), b is the width of the sample (mm) and h is the thickness of the sample (mm).

$$\varepsilon_c = \frac{6\, s\, h}{{L_2}^2} \tag{3}$$

ε_c is the apparent strain of a curved sample subjected to bending before the curvature correction (mm/mm), s is the displacement of the surface of the sample at the point of the load application from its initial position (mm):

$$E_c = \frac{\sigma_{c2} - \sigma_{c1}}{\varepsilon_{c2} - \varepsilon_{c1}} \tag{4}$$

where E_c is the apparent bending modulus of a curved sample subjected to bending before the curvature correction (MPa), σ_{c2} is the apparent stress at point 2 (MPa), σ_{c1} is the apparent stress at point 1 (MPa), ε_{c2} is the apparent strain at point 2 (mm/mm), and ε_{c1} is the apparent strain at point 1 (mm/mm).

Finally, the curvature correction coefficients C_σ Eq. (5) and C_E Eq. (7) were calculated. Then, Eq. (6) and Eq. (8) were applied according to EN ISO 11296–4 [10], to calculate the flexural modulus (E_f) and the flexural stress (σ_f):

$$C_\sigma = \frac{1 + \frac{h}{6R_2}}{cos\ \phi} \tag{5}$$

where C_σ is the curvature correction coefficient, R_2 is the radius of curvature of the sample at the average sample thickness, and ϕ is the half angle of an unloaded sample formed between the real contact points of the supports (see Fig. 9). In the tests performed, a value of $\phi = 0.258$ rad ($\phi = 14,8^{\circ}$) was used, obtaining $C_\sigma = 1.039$.

$$\sigma_f = \frac{\sigma_c}{C_\sigma} \tag{6}$$

σ_f is the flexural stress of a flat sample subjected to bending loads (MPa).

$$C_E = \frac{\left(\frac{L_2}{2R_2}\right)^3 cos^2\phi}{1,5\left[\phi - \left(\frac{L_2}{2R_2}\right) cos\ \phi\right]} \tag{7}$$

C_E is the curvature correction coefficient for the flexural modulus.

$$E_f = \frac{E_c}{C_E} \tag{8}$$

E_f is the flexural modulus of a flat sample subjected to bending loads (MPa).

4.4. Digital Image Correlation setup

A 3D Digital Image Correlation (DIC) system was used during the three-point bending tests to analyze the strain distribution along the thickness of the CIPP samples. To create the speckle pattern, the samples were airbrushed with different tip diameters (see Fig. 10). Two Allied Vision GigE MAKO G-507B GigE cameras with APO-Xenoplan 1.4/23–0903 objectives were used to record the surface displacement of the samples. Calibration was performed with a GOM CP20/MV55×44 panel with an offset of 0.021 pixels. The measurement volume resulting from the calibration was 150 × 130 × 110 mm. Finally, the image sequences were post-processed with GOM Correlate Professional software using a facet size of 12 × 12 pixels.

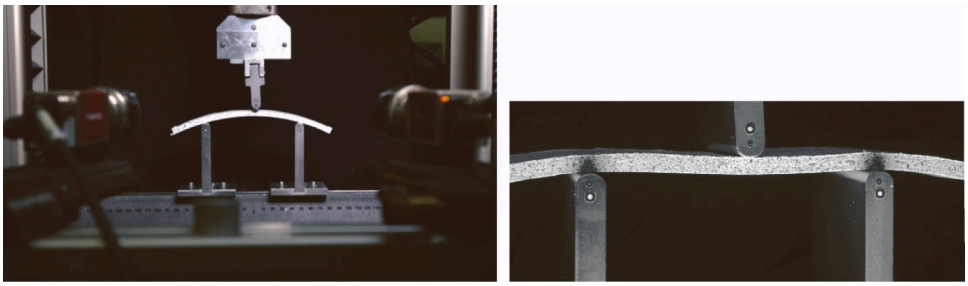

Fig. 10. Digital Image Correlation setup used during the three-point bending test of curved samples.

4.5. Inner Balloon Pressure Test

To experimentally validate the proposed test, a 600 × 600 mm prototype (Fig. 5) was designed and built (Fig. 11) to test samples up to DN500 mm. The prototype consisted of two rigid plates reinforced with 6 IPN 100 (S275JR) steel beams joined with M16 threaded rods. A Wika pressure sensor type A-10 was used to monitor the pressure. HBM strain gauges type 1-LY41–6 / 350 were used in the hoop direction to measure the hoop strain during the test. HBM's Quantum X MX840 B and Quantum X MX1615 B hardware and CatmanEasy AP software were employed for data acquisition. The prototype was used to test both PVC and cured CIPP liner samples from an installed liner. The PVC sample had a nominal diameter of 240 mm, a thickness of 5 mm, and a length of 80 mm. The CIPP liner ring sample had a nominal diameter of 385 mm, a length of 80 mm, and an average thickness of 6 mm (Fig. 11).

4.6. Numerical models

A static structural implicit Ansys model was created to model the tensile performance of flat and ring samples. Due to the symmetry of both sample geometries, simulations were performed using half of the sample (Fig. 12). For the tensile sample, the ASTM D638 [36] type I standard test geometry was meshed using higher-order 3-D 10-node (Solid 187) 3 mm elements size. A type 1 refinement was applied to the area where the stress concentration was located. The mesh had 8909 nodes. Fixed support was set on the sample's lower face (xz plane) to simulate the effect of the grips in the experimental test. A displacement of 5 mm on the y-axis was defined on the upper face of the sample. The material's mechanical properties were obtained by applying true stress compensation to the data acquired from the experimental tensile-strength test. Finally, the plastic region was defined by the hardening isotropic multilinear plasticity option.

The IBPT numerical models' geometry was different for each material. Ring PVC model had a DN of 240 mm, a thickness of 5 mm, and a length of 80 mm. Ring CIPP model had a DN of 385 mm, a thickness of 6 mm, and a length of 80 mm. Ring geometries were meshed using higher-order 3-D 20-node (Solid 186) 10 mm elements size. The properties of the materials were defined according to the Ansys data base and completed with the results of the experimental tensile tests for each material. The CIPP liner used had a Young modulus of 20.5 GPa, a Poisson's ratio of 0.1543 a shear modulus of 8.9 GPa and a density of 1857 kg/m^3. On the other hand, the PVC used had a Young modulus of 3.4 GPa, a Poisson's ratio of 0.4 a shear modulus of 1.2 GPa and a density of 1392 kg/m^3. For both models, a frictionless support was defined on the semicircular section (YZ plane) and two frictional supports of $\mu = 0.05$ on the top and bottom face of the ring (XY plane). Next, two remote displacements were set. The first remote displacement was defined at 3 and 9 o′clock in the YZ plane to avoid x-displacement and z-rotation. The second remote displacement was defined at 12 o′clock in the XZ plane to suppress the y-displacement and z-rotation (Fig. 12). Finally, the total stress and strain curves in the hoop direction were obtained.

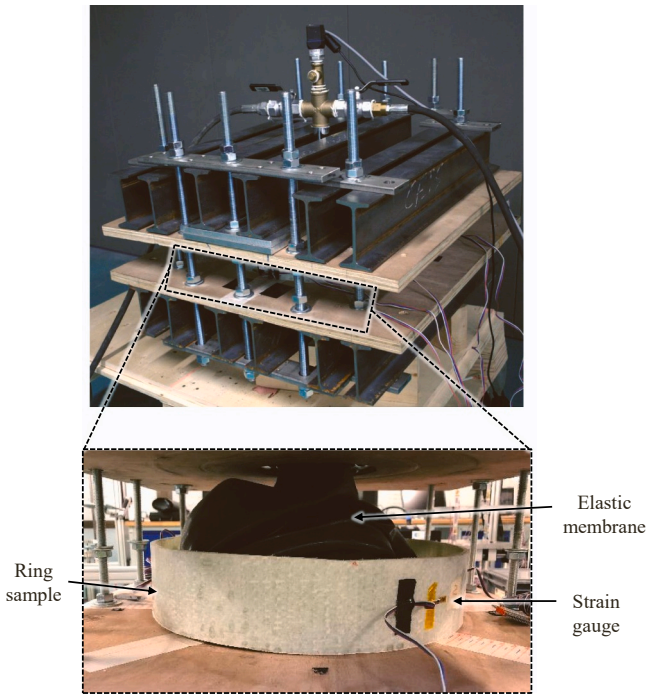

Fig. 11. Inner Balloon Pressure Test setup.

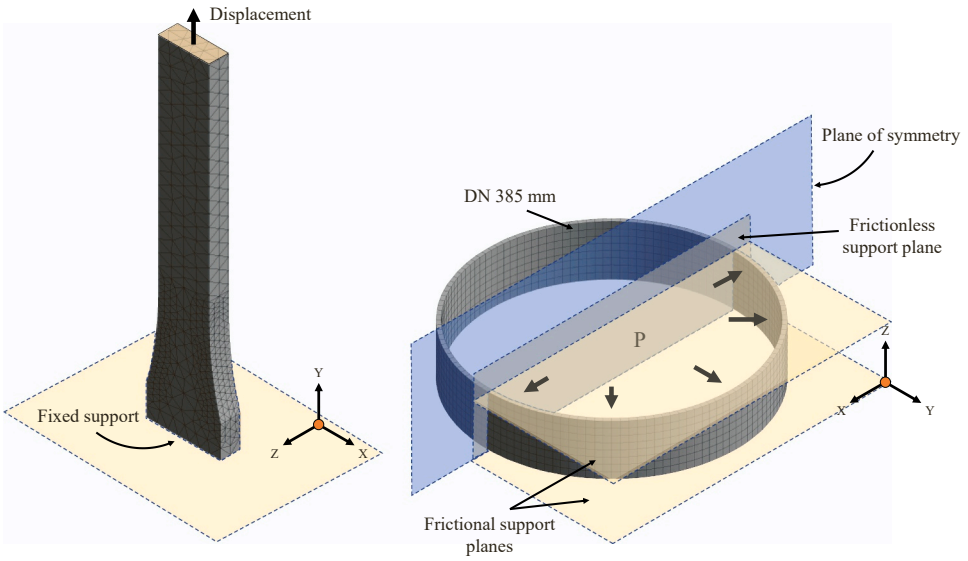

Fig. 12. Numerical model geometry of the tensile strength test ASTM D638 (left) and the Inner Balloon Pressure Test (right).

5. Results and discussion

5.1. Comparison between the bending and tensile test performance

During the three-point bending test, three failure modes were identified, as shown in Fig. 13. Among them, compressive failure due to buckling of the top layer fibers (Fig. 13a), and delamination failure (Fig. 13b) due to shear stresses are undesirable phenomena when trying to determine the tensile strength of the composite material. Only the failure of the outer layer due to tensile stress (Fig. 13c) is expected to occur under the operational conditions of the CIPP liner. The variety of failure modes demonstrates that the mechanical phenomena along the sample thickness are complex because a combination of tensile, compressive and shear stresses are given simultaneously.

Fig. 14 compares the results of the tensile strength test of flat CIPP samples to the three-point bending test of CIPP curved samples. As shown, the stress-strain curves differ markedly between the two tests, despite the samples being manufactured using the same material. Stress and strain at break obtained in the bending test according to standard EN ISO 11296–4 [10] are up to three times higher than those obtained on the tensile ASTM D638 test [36]. Hence, experimental evidence suggests that the obtained values from the bending test may not represent the ultimate stress of the CIPP liner. Since strength is a parameter used in the design of the liner, this finding could negatively affect the structural safety of the installed liner.

An incorrect assumption of a linear strain distribution inside the liner could explain the aforementioned result. To validate this hypothesis, Fig. 15 depicts the strain distribution along the sample thickness in the bending test obtained by the DIC results. The strain distribution is represented at two instances during the test. The first state corresponds to the external layer of the sample reaching the composite's ultimate strain measured in the tensile test. The second is the state just before failure when the fiber-resin region reaches the maximum strain of the composite measured in the tensile test.

As shown in Fig. 15, the DIC system shows at both states a linear strain distribution along the thickness of the sample, demonstrating the validity of the linear strain distribution model described by the equations in EN ISO 11296–4 [10].

Fracture propagation was also examined (see Fig. 16). In the three-point bending test, the outermost layer of the specimen is subjected to the highest tensile stress, meaning the fracture starts in the outer layer and propagates inwards. Fig. 16(a) shows the phenomenon. For clarity, Fig. 16b) shows the same failure mechanism using a 30 mm thick liner. In both cases, the fracture originated just after the polymer coating at the beginning of the resin-fiber region and propagated inwards. This phenomenon occurs because the

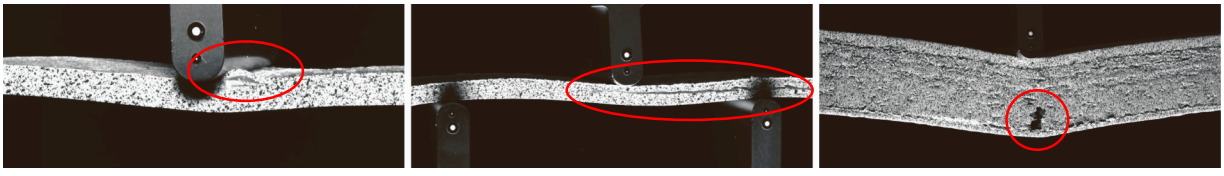

Fig. 13. Types of failure modes identified in the three-point bending test of CIPP composite liner: a) Compressive failure due to buckling of the upper fiber. b) Delamination of layers. c) Failure of the external layer due to tensile stress.

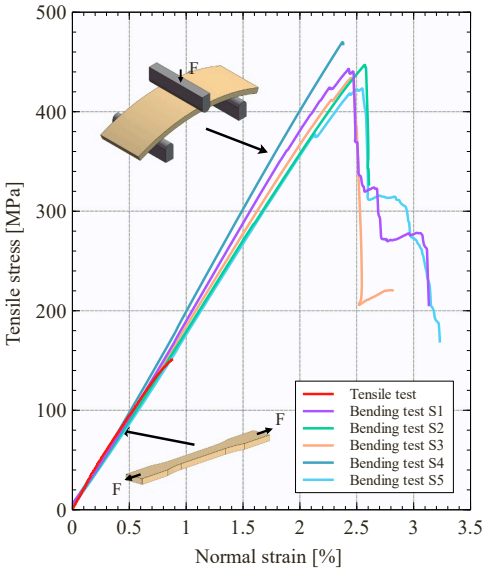

Fig. 14. Comparison between results of tensile strength of flat CIPP samples and three-point bending CIPP curved samples. The ultimate stress obtained with the bending test is up to three times higher than in the tensile test.

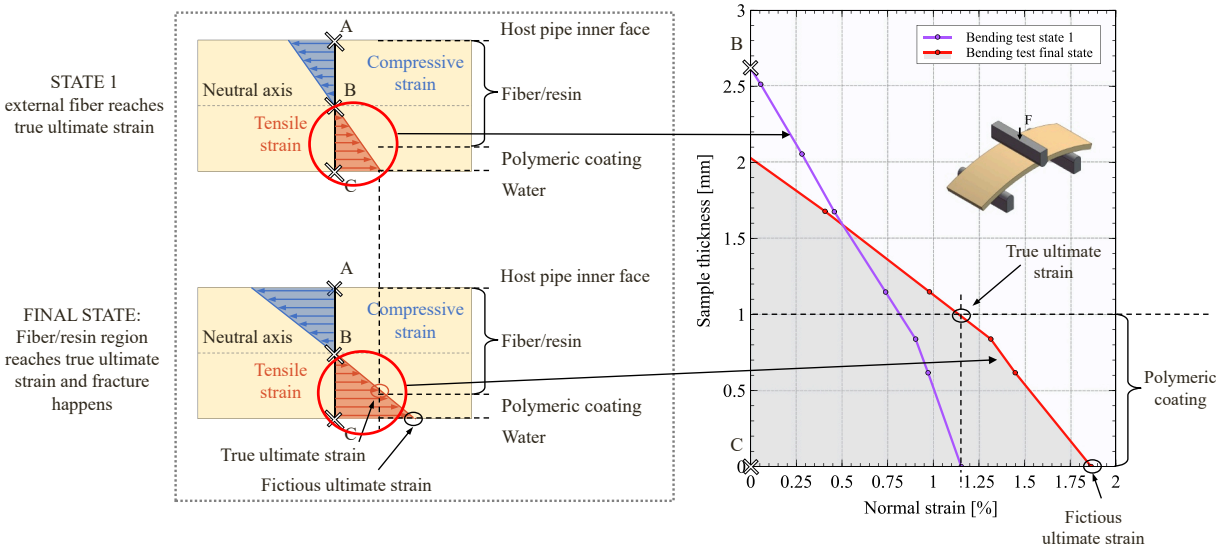

Fig. 15. Through-thickness strain distribution of a three-point bending test at two instants measured by experimental Digital Image Correlation.

outermost layer of the sample consists of a polymer coating with a ductile behavior. Therefore, even if the strain-to-rupture limit of the composite is reached (state 1, Fig. 15), the polymer layer continues to deform. Thus, failure (final state, Fig. 15) occurs in the inner zone adjacent to the polymer layer when the composite reaches its tensile limit. The thickness of the polymer coating was approximately 1 mm.

Fig. 15 (right) shows that, in the final state, the slope change in the strain distribution occurs around 1 mm from the bottom face, corresponding to the crack location. Moreover, the strain determined is similar to the ultimate strain of the composite obtained in the tensile test of the flat specimens (1.15% and 0.89%, respectively).

5.2. Inner Balloon Pressure Test validation

5.2.1. Numerical analysis: friction effect and tensile performance

As a preliminary step to the validation of the test, a numerical analysis was performed to analyze the boundary conditions of the IBPT and verify its performance as a tensile test of ring samples. The analysis is carried out on PVC samples as their well-determined

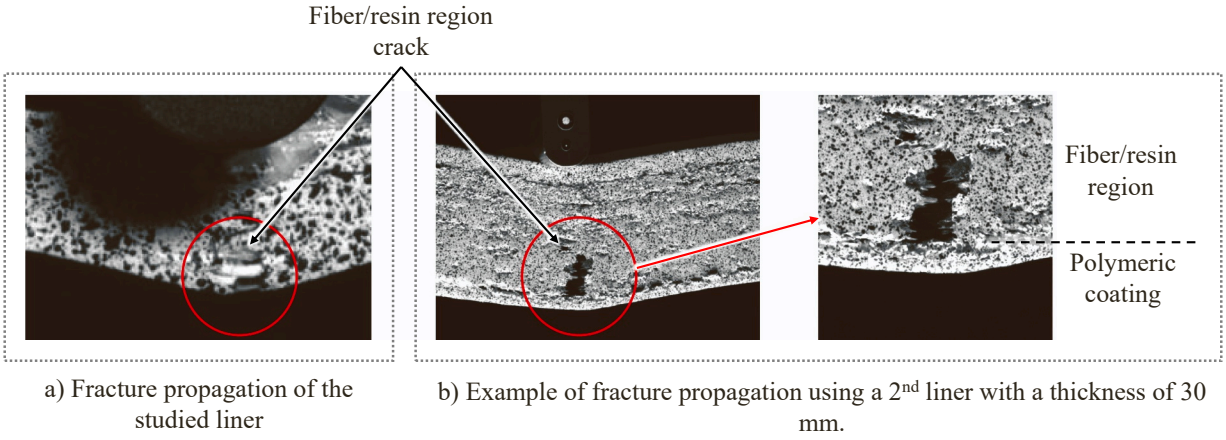

Fig. 16. Crack propagation analysis of the three-point bending test of CIPP liners experimentally observed by Digital Image Correlation.

properties allow the numerical model to be calibrated.

Initially, the ring sample is in contact with the upper and lower plates of the tooling (Fig. 5). Therefore, a frictional contact appears that could negatively affect the results and the performance of the test. Considerable friction ($\mu = 1$) would bend the sample into a barrel shape, as shown in Fig. 17, generating longitudinal stresses and causing problems with the inner membrane of the tooling (Fig. 11). However, the use of lubricant and the nature of the IBPT prevent the appearance of friction effect. During the test, the inner membrane also exerts pressure on the tooling's lower and upper plates, generating a gap between both plates and the test sample. In addition, the longitudinal shrinkage caused by the Poisson effect increases the gap between the tooling covers and the sample. Thus, the ring sample can expand with a minimum friction coefficient, and the barrel shape of the sample represented in Fig. 17 is discarded.

The stress-strain curves of PVC samples obtained using the IBPT model (II) and the ASTM D638 [36] tensile test numerical model (I) are represented in Fig. 18. IBPT results have been obtained assuming a friction coefficient of $\mu = 0.05$. As shown, the IBPT model presents a tensile behavior in agreement with the flat sample tensile test, identifying an error under the curve of 0.25%. Hence, the results demonstrate that the IBPT can reproduce the tensile stress performance with ring samples analogous to the tensile test.

5.2.2. *Validation results on PVC samples*

Fig. 19 shows the results obtained from PVC samples for the experimental validation of the IBPT. The graph compares a representative stress-strain curve of the tensile test (V) (ASTM D638 [36]) with the numerical (IV) and experimental (I, II and III) IBPT results. In the experimental IBPT, the results of the three strain channels corresponding to the three strain gauges installed on the outer surface of the specimen are plotted. As shown, these strain results display a similar trend. For example, the strain at 15 bar was 1.29% (channel 1), 1.51% (channel 2) and 1.16% (channel 3). The differences (0.18% standard deviation) between the channels are attributed to small misalignments in the placement and alignment of the strain gauges during installation. Consistent results are also concluded from the experimental tensile test (V) and the numerical simulation (IV).

In contrast, more variation is observed between the IBPT experimental curves (I, II and III) and the tensile test (V). The maximum deformation average reported by the three channels of the IBPT was 3.06%, while a maximum deformation of 8% was reached in the standard tensile test of flat specimens. This significant decrease in strain (161%) and increase in stress (6.39%) is attributed to the difference in load rate during the test [38]. In the IBPT, the pressure rate was controlled manually to increase the balloon's internal pressure. However, the control of the inlet pressure was not sufficiently gradual, which occasionally caused the material in the plastic zone to tear instead of yield. This tearing phenomenon can be seen in Fig. 19 by observing the wavy lines at the end of the curves in the experimental IBPT (I, II and III). In contrast, the tensile test was performed according to ASTM D638 [36], with a constant loading rate controlled by the hardware of the test equipment. Aside from this difference, the IBPT allows for a reliable reproduction of the working conditions of the ring specimens, permitting the assessment of the mechanical performance as an alternative to the tensile and flexural classical tests.

5.2.3. *Validation results on CIPP composite samples*

Fig. 20 shows the IBPT experimental stress-strain results (curves I and II), and a representative tensile test curve (III) of a flat specimen. Both tests used CIPP composite specimens. As in the previous section, the IBPT results reveal that the specimen could expand freely in the hoop direction. However, the results show differences in ultimate stresses. In both tests, the ultimate strain was consistent (tensile test 0.89%, IBPT ch1 0.77%, IBPT ch2 1.03%). However, the IBPT shows a higher ultimate stress ($\sigma_u = 201.4$ MPa, 1.34 times) compared to the ultimate stress of the tensile test ($\sigma_u = 150.9$ MPa). The type of curing process of the specimens could explain this phenomenon of non-correlation of ultimate strength.

In the IBPT, the specimens were taken from an installed liner and cured with internal pressure by a certified installer. In contrast, the flat specimens were cured in the laboratory, in an attempt to reproduce the conditions of the certified equipment but without pressure. The SEM microscopy images in Fig. 21 show that the cross-section of a sample of the installed liner (d, e and f) does not show

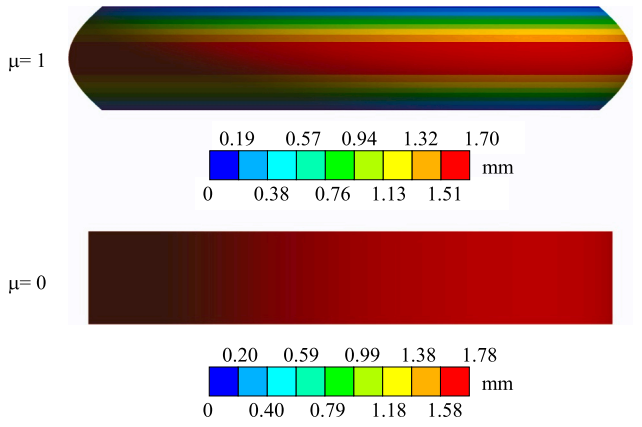

Fig. 17. Adjustment of the friction boundary conditions of the IBPT numerical model.

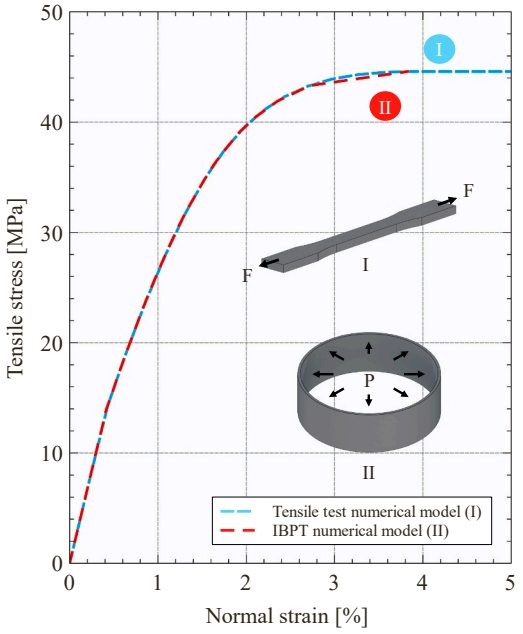

Fig. 18. Comparison between the stress-strain numerical results of the tensile and IBP PVC sample tests.

any defects, which guarantees good compaction of the laminate. In contrast, the samples cured in the laboratory (a, b and c) show defects indicating an apparent absence of resin. This defect during curing is attributed to the absence of compaction pressure and is considered responsible for the decrease in the mechanical properties of the flat samples.

Finally, Fig. 22 compares representative stress-strain curves obtained from the three-point bending test of curved specimens, the experimental IBPT of ring specimens and the tensile test of flat specimens. The graph on the right shows the magnified data of the first third of the curve. Overall, a good correlation is found in the stiffness of the specimens: $E_{flexural} = 21.1$ GPa ($E_c = 19.3$ GPa before curvature correction, see Eqs. (7) and (8), $E_{tensile} = 20.5$ MPa and $E_{IBPT} = 21.2$ GPa. According to the standard test, stiffnesses have been calculated on the strain range [0.05–0.25%].

However, as anticipated, a significant difference is recognized in the ultimate stress. The burst pressure obtained from the tensile test should not be considered as it was influenced by the aforementioned impregnation defects. As shown, the burst pressure obtained from the bending test of curved specimens is 138.2 bar (443.4 MPa), which is greater than twice the 62.8 bar (201.4 MPa) obtained in the IBPT. It should be noted that both samples were taken from the same installed liner. Hence, this experimental evidence highlights once again the possible unsuitability of the bending test to characterize the behavior of CIPP composite liners.

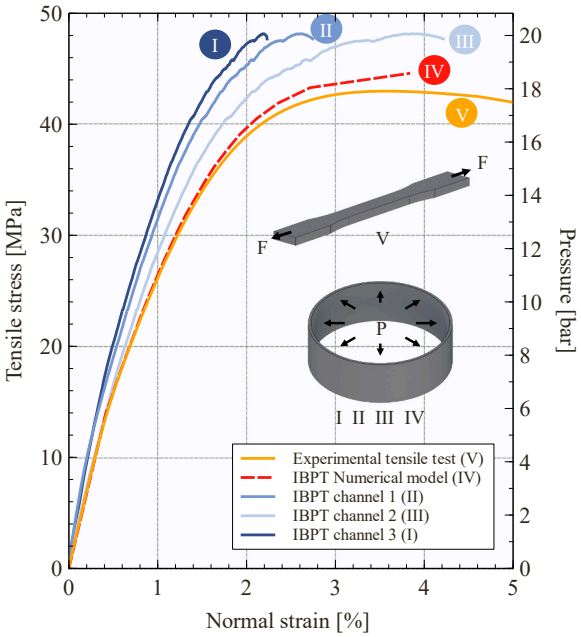

Fig. 19. Validation of the IBP test with PVC samples.

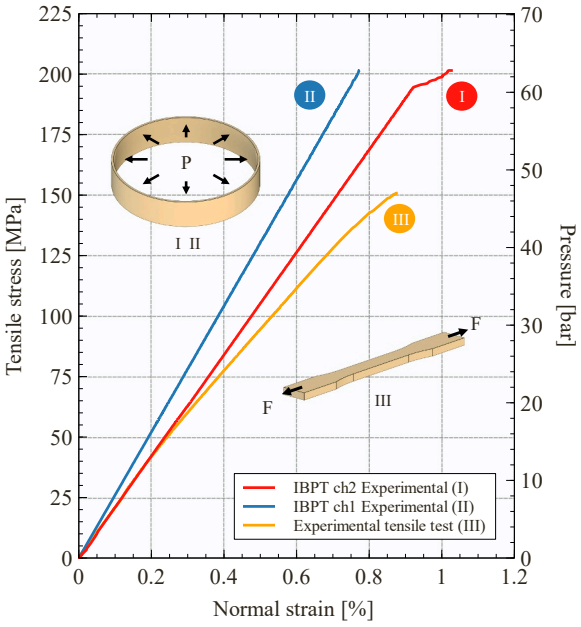

Fig. 20. Validation of the IBP test with CIPP composite samples.

6. Conclusions

This paper proposes and validates the Inner Balloon Pressure Test, a new test procedure for the quality control of CIPP rehabilitation liners. The test aims to reproduce the working stress conditions of an installed CIPP liner to evaluate its hoop tensile strength. Although the traditional tensile test should be the most suitable test to assess the tensile properties of an installed liner due to its operational simplicity, the impracticality of extracting flat specimens in the hoop direction from an installed cylindrical liner makes the tensile test unfeasible. Consequently, current CIPP standards EN ISO 11296–4 [10] and ASTM F1216 [9] suggest using the three-point bending test to assess the hoop tensile performance of an installed liner. However, experimental evidence indicates that the bending test of curved samples overestimates the ultimate stresses of a cured CIPP liner by more than two times. Hence, the IBPT on ring

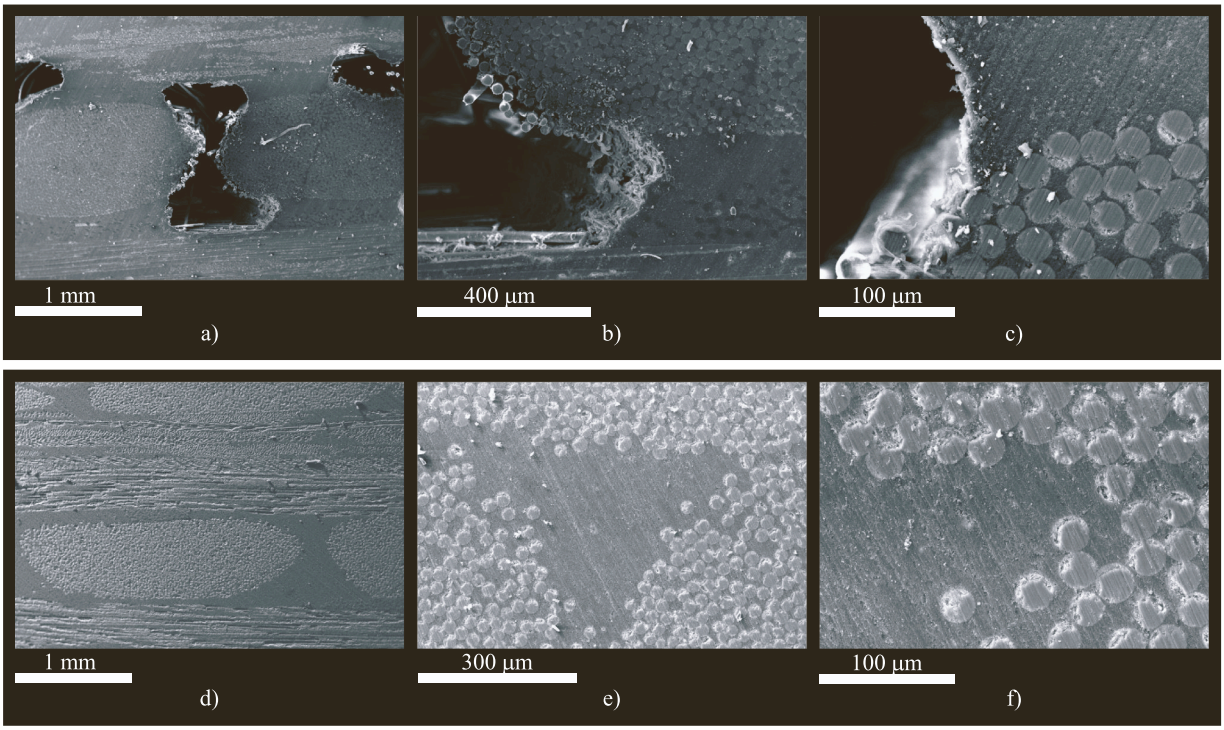

Fig. 21. Comparison of SEM microscopy images of the cross-section of a sample cured in laboratory conditions without compression pressure (a, b, and c), and cured by a certified installer with internal pressure (d, e, and f).

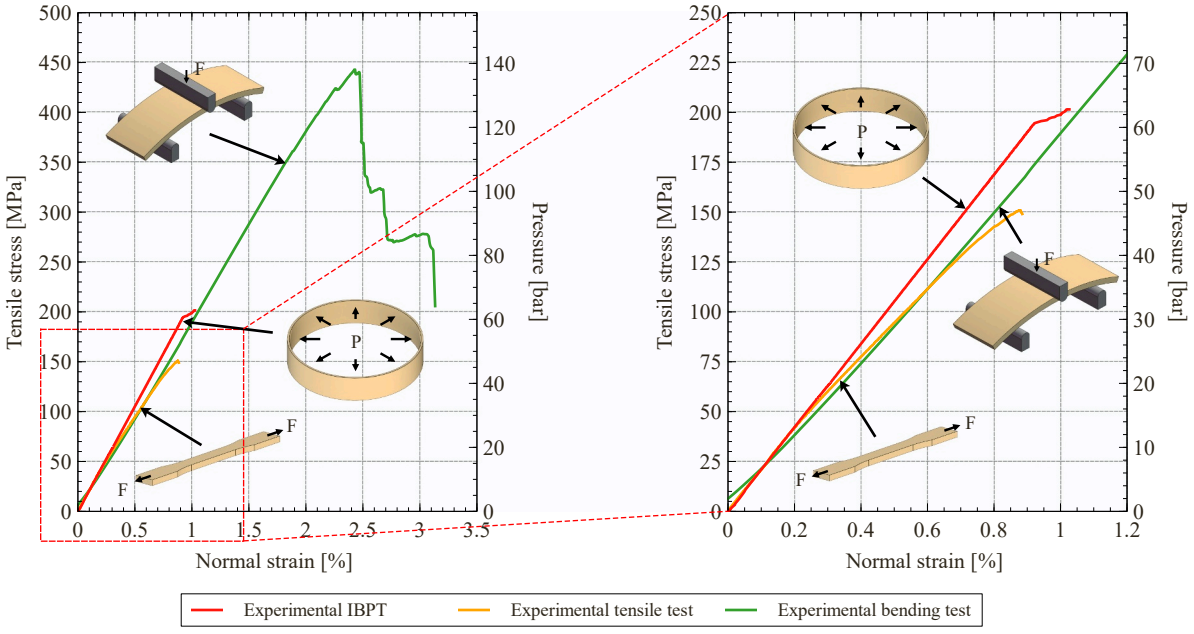

Fig. 22. Comparison between tensile, bending and IBPT of CIPP composite tests results.

samples is proposed as an alternative to the curved specimen bending test recommended by current CIPP standards. The proposed IBPT effectively addresses the limitations detected in the three-point bending test conducted on curved specimens. Furthermore, it provides a solution to the challenge of extracting flat samples in the hoop direction for the tensile test, as the IBPT is performed on ring samples, which can be easily cut on-site after the liner has been installed. Furthermore, the experimental results obtained with the IBPT show a high correlation with the flat specimen tests.

The experimental evidence provided in this study have a significant impact on the design of CIPP pressure pipe liners. Inadequate sizing of the structural reinforcement can compromise the functionality of the liner and the rehabilitation of the pipeline. Assuming a strength value higher than the actual strength of the liner means reducing the thickness required for rehabilitation. It is important to note that the relationship between the obtained burst pressure overestimates is close to the sizing safety coefficients. On the other hand, an oversizing of the liner increases the complexity of the installation, reduces its maneuverability, and requires a higher installation pressure. It also increases the likelihood of installation defects. Therefore, the repair or replacement of the rehabilitated pipe with installation defects may involve a higher cost than the initial replacement.

For all these reasons, correct sizing and quality control through representative tests increase the reliability of the rehabilitation system, reducing the uncertainties that limit the applicability of this technology. Consequently, the IBPT is a relevant contribution to the quality control of the CIPP industry. Therefore, this study provides a novel test that reduces the uncertainties related to the strength analysis of CIPP liners. Furthermore, it contributes to the optimization and advancement of existing design and quality control tests.

Declaration of Competing Interest

The authors declare that they have no known competing financial interests or personal relationships that could have appeared to influence the work reported in this paper.

Data availability

Data will be made available on request.

Acknowledgments

The authors would like to gratefully acknowledge the financial support provided by Agència de Gestió d'Ajuts Universitaris i de Recerca and the Pla de Doctorats Industrials del Department de Recerca i Universitats de la Generalitat de Catalunya with reference project 2019 DI45. The authors also appreciate the collaboration of companies SAERTEX multiCom Group and Aquatec S.A. for contributing materials, data, and services. Finally, a special mention to Ludwing Felipe Libreros from Aquatec S.A. and Timo Münstermann from SAERTEX multiCom Group.

References

[1] M.V. Seica, J.A. Packer, M.W. Grabinsky, B.J. Adams, Evaluation of the properties of Toronto iron water mains and surrounding soil, Can. J. Civ. Eng. 29 (2) (2002) 222–237, https://doi.org/10.1139/l01-090.
[2] ASCE (American Society of Civil Engineers), A Comprehensive Assessment of America's Infrastructure, Tech. rep., 2021.
[3] AEAS, AGA, XVI Estudio nacional de suministro de agua potable y saneamiento en España 2020, Tech. rep., Spain, 2020.
[4] E. Renaud, A. Husson, A. Vacelet, Y. LeGat, A.E. Stricker, Statistical modelling of French drinking water pipe inventory at national level using demographic and geographical information, H2Open J. 3 (1) (2020) 89–101, https://doi.org/10.2166/h2oj.2020.028.
[5] C. Berger, C. Falk, F. Hetzel, J. Pinnekamp, J. Ruppelt, P. Schleiffer, J. Schmitt, Zustand der Kanalisation in Deutschland: Ergebnisse der DWA-Umfrage 2020, KA Korresp. Abwasser Abfall 67 (12) (2020) 939–953, https://doi.org/10.3242/kae2020.12.001.
[6] Stratview Research Cured-In-Place Pipe (CIPP) Market by Pipe Diameter Type, by Resin Type, by Fabric Type, by Cure Type, by Weaving Type, by Coating Type, and by Region, Trend, Forecast, Competitive Analysis, and Growth Opportunity: 2018–2023, Tech. rep., 2018.
[7] S. Khan, C. Dobson, Trouble shooting for trenchless liner installation during sewer line rehabilitation, In: Proceedings of the Water Environment Federation, Vol. 1, Sacramento, California, 2006, pp. 5420–5435. ⟨10.2175/193864706783763192⟩.
[8] S. Das, A. Bayat, L. Gay, M. Salimi, J. Matthews, A comprehensive review on the challenges of cured-in-place pipe (CIPP) installations, J. Water Supply. Res. Technol. AQUA 65 (8) (2016) 583–596, https://doi.org/10.2166/aqua.2016.119.
[9] ASTM F1216, Standard Practice for Rehabilitation of Existing Pipelines and Conduits by the Inversion and Curing of a Resin-Impregnated Tube, ASTM International, West Conshohocken, PA, 2022. ⟨www.ASTM.org⟩.
[10] EN ISO 11296–4, Plastics Piping Systems for Renovation of Underground Non-pressure Drainage and Sewerage Networks - Part 4: Lining with Cured-in-place Pipes, 2018. ⟨www.iso.org⟩.
[11] ISO 11298–4, Plastics Piping Systems for Renovation of Underground Water Supply Networks – Part 4: Lining with Cured-in-place Pipes, 2021. ⟨www.iso.org⟩.
[12] H. Zhu, T. Wang, Y. Wang, V.C. Li, Trenchless rehabilitation for concrete pipelines of water infrastructure: a review from the structural perspective, Cem. Concr. Compos. 123 (2021), 104193, https://doi.org/10.1016/j.cemconcomp.2021.104193.
[13] UNE-EN ISO 11298–4, Sistemas de canalización en materiales plásticos para la renovación de redes de conducción de agua enterradas. Parte 4: Entubado continuo con tubo curado en obra, 2022. ⟨www.iso.org⟩.
[14] UNE 53929, Plásticos. Rehabilitación de conducciones de abastecimiento y alcantarillado con tubos continuos curados in situ (CIPP).Diseño, cálculo e instalación, 2022. ⟨www.une.org⟩.
[15] E.N. Allouche, G. Shanghai, M. Baumert, A. Amobi, K. Bainbridge, The design and performance of pressure pipe liners under static and cyclic loading, In: Proceedings of the Pipelines Congress 2008 – Pipeline Asset Management: Maximizing Performance of Our Pipeline Infrastructure, 321, 2008, pp. 1–10. ⟨10.1061/40994(321)38⟩.
[16] E.N. Allouche, K. Bainbridge, I.D. Moore, H.C. Council, Laboratory Examination of a Cured In Place Pressure Pipe Liner for Potable Water Distribution System, In: NASTT, No-Dig 2005, Vol. 13689, Orlando, Florida, 2005, pp. 1–10.
[17] A. Jaganathan, E. Allouche, M. Baumert, Experimental and numerical evaluation of the impact of folds on the pressure rating of CIPP liners, Tunn. Undergr. Space Technol. 22 (5–6) (2007) 666–678, https://doi.org/10.1016/j.tust.2006.11.007.
[18] Z. Yahong, H. Sheng, M. Baosong, Z. Cong, Y. Xuefeng, T. Zhongsen, L. Han, D. Caiying, Experiment and evaluation model of liner design for renewal of deteriorated reinforced concrete pipes utilizing cured-in-place-pipe technology, Tunn. Undergr. Space Technol. 132 (2023), https://doi.org/10.1016/j.tust.2022.104866.
[19] ASTM F2207, Standard Specification for Cured-in-Place Pipe Lining System for Rehabilitation of Metallic Gas Pipe, ASTM International, West Conshohocken, PA, 2019. ⟨www.astm.org⟩.
[20] N. Ampiah, A. Fam, I.D. Moore, Effect of wrinkles on the circumferential strength of a cast-in-place composite polymer liner used in retrofitting pressure pipes, J. Mater. Civ. Eng. 22 (12) (2010) 1304–1314, https://doi.org/10.1061/(ASCE)MT.1943-5533.0000160.

[21] N. Ampiah, A. Fam, I.D. Moore, Wavy imperfections and the strength of cast-in-place pressure pipe liners, In: Proceedings of the Pipelines Congress 2008 – Pipeline Asset Management: Maximizing Performance of Our Pipeline Infrastructure, 321, 2008. ⟨10.1061/40994(321)54⟩.
[22] E. Allouche, S. Alam, J. Simicevic, R. Sterling, W. Condit, J. Matthews, A. Selvakumar, A pilot study for retrospective evaluation of cured-in-place pipe (CIPP) rehabilitation of municipal gravity sewers, Tunn. Undergr. Space Technol. 39 (2014) 82–93, https://doi.org/10.1016/j.tust.2012.02.002.
[23] K. Yang, H. Fang, J. Bu, X. Zhang, B. Li, X. Du, Z. Zhang, Full-scale experimental investigation of the mechanical characteristics of corroded buried concrete pipes after cured-in-place-pipe rehabilitation, Tunn. Undergr. Space Technol. 117 (2021), 104153, https://doi.org/10.1016/j.tust.2021.104153.
[24] K. Yang, H. Fang, X. Zhang, B. Li, Q. Hu, Investigation of mechanical properties of corroded concrete pipes after cured-in-place-pipe (CIPP) rehabilitation under multi-field coupling, Tunn. Undergr. Space Technol. 128 (2022), https://doi.org/10.1016/j.tust.2022.104656.
[25] J.M. Hsu, K.J. Shou, Experimental study of the separated joint of an underground pipeline rehabilitated by cured-in-place pipe, Undergr. Space 7 (4) (2022) 543–563, https://doi.org/10.1016/j.undsp.2021.11.005.
[26] J.A. Hudson, H. Cardenas, J. Matthews, S. Alam, Performance evaluation of deteriorated and rehabilitated corrugated metal pipe culverts using multiphysics simulation, Tunn. Undergr. Space Technol. 131 (2022) (2023), 104827, https://doi.org/10.1016/j.tust.2022.104827.
[27] T. Abel, Laboratory tests and analysis of CIPP epoxy resin internal liners used in pipelines-part II: comparative analysis with the use of the FEM and engineering algorithms, Stud. Geotech. Mech. 43 (3) (2021) 307–322, https://doi.org/10.2478/sgem-2021-0007.
[28] X. Sun, M. He, Z. Li, Novel engineered wood and bamboo composites for structural applications: State-of-art of manufacturing technology and mechanical performance evaluation, Constr. Build. Mater. 249 (1239) (2020), 118751, https://doi.org/10.1016/j.conbuildmat.2020.118751.
[29] N.M. Nurazzi, M.R. Asyraf, S. FatimahAthiyah, S.S. Shazleen, S.A. Rafiqah, M.M. Harussani, S.H. Kamarudin, M.R. Razman, M. Rahmah, E.S. Zainudin, R. A. Ilyas, H.A. Aisyah, M.N. Norrrahim, N. Abdullah, S.M. Sapuan, A. Khalina, A review on mechanical performance of hybrid natural fiber polymer composites for structural applications, Polymers 13 (13) (2021) 1–47, https://doi.org/10.3390/polym13132170.
[30] Z. Kamble, B.K. Behera, Sustainable hybrid composites reinforced with textile waste for construction and building applications, Constr. Build. Mater. 284 (2021), 122800, https://doi.org/10.1016/j.conbuildmat.2021.122800.
[31] W. Fan, W. Dang, T. Liu, J. Li, L. Xue, L. Yuan, J. Dong, Fatigue behavior of the 3D orthogonal carbon/glass fibers hybrid composite under three-point bending load, Mater. Des. 183 (2019), 108112, https://doi.org/10.1016/j.matdes.2019.108112.
[32] X. Guijun, G. Rui, L. Chenggao, Combined effects of sustained bending loading, water immersion and fiber hybrid mode on the mechanical properties of carbon/glass fiber reinforced polymer composite, Compos. Struct. 281 (2022), 115060, https://doi.org/10.1016/j.compstruct.2021.115060.
[33] Y. Xia, M. Shi, C. Zhang, C. Wang, X. Sang, R. Liu, P. Zhao, G. An, H. Fang, Analysis of flexural failure mechanism of ultraviolet cured-in-place-pipe materials for buried pipelines rehabilitation based on curing temperature monitoring, Eng. Fail. Anal. 142 (2022), 106763, https://doi.org/10.1016/j.engfailanal.2022.106763.
[34] AWW Committee Report, Structural Classifications of Pressure Pipe Linings, Suggested Protocol for Product Classification, Tech. rep., 2019.
[35] ISO 11295, Classification and Information on Design and Applications of Plastics Piping Systems Used for Renovation and Replacement, 2018. ⟨www.iso.org⟩.
[36] ASTM D638, Standard Test Method for Tensile Properties of Plastics, ASTM International, West Conshohocken, PA, 2022. ⟨www.ASTM.org⟩.
[37] ISO 178, Determination of Flexural Properties Plastics – Determination of Flexural Properties, 2019. ⟨www.iso.org⟩.
[38] E.A. Campo. Selection of Polymeric Materials: How to Select Design Properties from Different Standards, first ed., William Andrew, 2008.